THE JOURNAL OF BIOLOGICAL CHEMISTRY VOL. 285, NO. 23, pp. 17771–17777, June 4, 2010

Golgi *N*-Glycosyltransferases Form Both Homo- and Heterodimeric Enzyme Complexes in Live Cells*

Received for publication, January 12, 2010, and in revised form, April 8, 2010 Published, JBC Papers in Press, April 8, 2010, DOI 10.1074/jbc.M110.103184

Antti Hassinen, Antti Rivinoja, Annika Kauppila, and Sakari Kellokumpu[1]

From the Department of Biochemistry, University of Oulu and the Glycoscience Graduate School Finland, P.O. Box 3000, Linnanmaa, FIN-90014 Oulu, Finland

Glycans (*i.e.* oligosaccharide chains attached to cellular proteins and lipids) are crucial for nearly all aspects of life, including the development of multicellular organisms. They come in multiple forms, and much of this diversity between molecules, cells, and tissues is generated by Golgi-resident glycosidases and glycosyltransferases. However, their exact mode of functioning in glycan processing is currently unclear. Here we investigate the supramolecular organization of the *N*-glycosylation pathway in live cells by utilizing the bimolecular fluorescence complementation approach. We show that all four *N*-glycosylation enzymes tested (*β*-1,2-*N*-acetylglucosaminyltransferase I, *β*-1,2-*N*-acetylglucosaminyltransferase II, 1,4-galactosyltransferase I, and *α*-2,6-sialyltransferase I) form Golgi-localized homodimers. Intriguingly, the same enzymes also formed two distinct and functionally relevant heterodimers between the medial Golgi enzymes *β*-1,2-*N*-acetylglucosaminyltransferase I and *β*-1,2-*N*-acetylglucosaminyltransferase II and the *trans*-Golgi enzymes 1,4-galactosyltransferase I and *α*-2,6-sialyltransferase I. Given their strict Golgi localization and sequential order of function, the two heterodimeric complexes are probably responsible for the processing and maturation of *N*-glycans in live cells.

Oligosaccharide chains attached to newly synthesized proteins and lipids in the endoplasmic reticulum (ER)[2] and the Golgi apparatus are known to play a crucial role in a variety of basic cellular functions and biological recognition events, including protein folding, membrane trafficking, cell signaling, binding of pathogens to host cells, immunological defense, fertilization, and embryonic development (1–4). Their functional importance is also highlighted by the recent identification of several glycosylation-associated disease states, such as congenital diseases of glycosylation, inflammation, and cancer (5–8).

The Golgi apparatus has multiple roles in glycosylation. It is responsible for the processing of ER-derived high mannose type *N*-glycans into hybrid and complex type *N*-glycans. In addition, it is responsible for the *de novo* synthesis of *O*-glycans, proteoglycans, and glycolipids. Its ability to correctly build all of these different glycoforms is thought to rely on its subcompartmentalization (9–12) and the distribution of glycosidases and glycosyltransferases within the different Golgi subcompartments in their expected order of function (13–16). However, it is still a mystery how the dozens of glycosylation enzymes that operate, frequently competitively, in the different Golgi glycosylation pathways are prevented from synthesizing irrelevant or mixed glycan structures. Interestingly, increasing *in vitro* evidence has indicated that glycosyltransferases tend to form oligomeric enzyme complexes in both yeast and mammalian cells (17–22). Complex formation was originally considered to provide only a means to correctly localize Golgi residents in the organelle (18, 23–25), but more recent evidence indicates that it may also increase the efficiency and accuracy of glycosylation reactions by physically linking relevant enzymes together (20). Thus, complex formation may help to create separate assembly lines, or pathways, for the synthesis of different glycoforms made by the organelle.

Direct evidence demonstrating that such assembly lines do indeed exist in live cells is very limited. This is mainly due to the fact that, in previous studies, complex formation has been traditionally assayed using *in vitro* pull-down assays. Furthermore, the ER retrieval approach, which has been used in live cells to detect complex formation between the medial Golgi enzymes GnTI, GnTII, and mannosidase II (EC 3.2.1.114), allows their detection only in the ER (23, 26, 27). Because the Golgi lumen is more acidic (pH 6.7–6.0) than that of the ER (pH 7.0–7.4) and Golgi acidity may affect complex formation (28–31), these two compartments may contain different enzyme complexes. In the present study, we have utilized the bimolecular fluorescent complementation (BiFC) approach (32) to screen potential interactions between Golgi *N*-glycosyltransferases for the first time in their native environment (*i.e.* the Golgi membranes of live cells). BiFC, which is based on the assembly of a fluorescent protein (*e.g.* YFP) from its non-fluorescent N- and C-terminal fragments, has been previously used to visualize interacting nuclear, cytoplasmic, and transmembrane proteins of the ER and the intermediate compartment (32–34). We show that all four of the main Golgi *N*-glycosyltransferases tested form either homodimers or functionally relevant heterodimers in live cells.

EXPERIMENTAL PROCEDURES

Plasmid Constructs—The original pCMV vector constructs were kindly donated to us by Dr. Hu (Purdue University). The plasmids contained sequences for the N-terminal hemaggluti-

* This work was supported by grants from the Academy of Finland, the University of Oulu, and the Finnish Glycoscience Graduate School.

[1] To whom correspondence should be addressed: Dept. of Biochemistry, University of Oulu, P.O. Box 3000, Linnanmaa, Door J, Rm. MN 212-1, FIN-90014 Oulu, Finland. E-mail: sakari.kellokumpu@oulu.fi.

[2] The abbreviations used are: ER, endoplasmic reticulum; VC, YFP_{Venus} C-terminal fragment; VN, YFP_{Venus} N-terminal fragment; SiaT, α-2,6-sialyltransferase I (EC 2.4.99.1); GalT, β-1,4-galactosyltransferase I (EC 2.4.1.38); GnTI, β-1,2-*N*-acetylglucosaminyltransferase I (EC 2.4.1.101); GnTII, β-1,2-*N*-acetylglucosaminyltransferase II (EC 2.4.1.143); BiFC, bimolecular fluorescence complementation; YFP, yellow fluorescent protein; TRITC, tetramethylrhodamine isothiocyanate; GFP, green fluorescent protein.

TABLE 1
cDNA clones, primers, and restriction enzymes used for the BiFC constructs

Transferase name	Abbreviation	Primer	Restriction enzyme
α(2,6)-Sialyltransferase I	SiaT, EC 2.4.99.1	Forward: 5′-AAAAAAAGCTTGAGGTCGGTACCATGATTC-3′	HindIII
		Reverse: 5′-AAAAATCTAGAGCAGTGAATGGTCCG-3′	XbaI
β(1,4)-Galactosyl-transferase I	GalT, EC 2.4.1.38	Forward: 5′-AAAAAAAGCTTCTCACCCCCAGGATG-3′	HindIII
		Reverse: 5′-AAAAATCTAGAGTGTGAACCTCGGAGGG-3′	XbaI
β-1,2-*N*-Acetylglucos-aminyltransferase I	GnTI, EC 2.4.1.101	Forward: 5′-AAAAAGGATCCATGCTGAAGAAGCAGTCTG-3′	BamHI
		Reverse: 5′-AAAAATCTAGAATTCCAGCTAGGATCATAGC-3′	XbaI
β-1,2-*N*-Acetylglucos-aminyltransferase II	GnTII, EC 2.4.1.143	Forward: 5′-AAAAAGAATTCCATGAGGTTCCGCATCTAC-3′	EcoRI
		Reverse: 5′-AAAAATCTAGACTGTGATTTCCACTGCAGTC-3′	XbaI

nin and FLAG epitope tags (cytoplasmic) followed by either the N-terminal (VN, residues 1–173) or the C-terminal (VC, residues 155–238) fragment of the YFP_{Venus} variant that is optimized for better folding at 37 °C (35). Expression of our first glycosyltransferase constructs (with C-terminally inserted SiaT) in COS-7 cells revealed that they accumulated in the ER (data not shown), probably due to their mislocalization (36). Therefore, we constructed new BiFC vectors by omitting both epitope tags, moderately extending the linker region of the VN construct, and placing the BiFC fragments (VN and VC) to the extreme C termini (luminal) of the enzyme constructs.

Briefly, VN and VC domains of the Venus variant were subcloned by PCR between the terminal XbaI and ApaI restriction sites of the pcDNA3 plasmid (Clontech). For the PCR, the following primer sets were used (VN, 5′-AAAAATCTAGAGCAGTCGACTTTAGAAGATCC-3′ (forward) and 5′-AAAAAGGGCCCCTACTCGATGTTGTGGCG-3′ (reverse); VC, 5′-AAAAATCTAGACCGGCGTGCAAAATC-3′ (forward) and 5′-AAAAAGGGCCCTTACTTGTACAGCTCGTCCATG-3′ (reverse). The original 5-amino acid linker region of the VN construct was lengthened to 12 amino acids (15 amino acids in the VC construct) by taking extra sequences from the original pCMV vector linker regions (32). The plasmid that encodes the full-length YFP Venus variant used as an interassay control was constructed by digesting the VN and VC PCR products with BstYI within their overlapping regions and combining the N- and C-terminal BiFC fragments by ligation before insertion into the XbaI and ApaI restriction enzyme cleavage sites of the pcDNA3 vector. Myc-tagged pcDNA3 vector was prepared by inserting annealed c-Myc epitope (10 amino acids)-specific primers (5′-CTAGAGAACAAAAACTCATCTCAGAAGGGATCTGTAGGGCC-3′ and 5′-CTACAGATCCCTTCTGAGATGAGTTTTTGTTCT-3′) into the XbaI and ApaI restriction enzyme cleavage sites of the pcDNA3 vector.

All glycosyltransferase constructs were prepared using sequence-verified, full-length cDNA clones (Imagenes GmbH, Berlin, Germany). After PCR amplification with specific primers (Table 1), each PCR product was digested before insertion, in-frame, with the XbaI restriction site of the vector constructs. The C24G mutant (31) of the human SiaT was prepared using the QuikChange II™ site-directed mutagenesis kit (Stratagene, La Jolla, CA) and primers designed with Stratagene's Web-based primer design program. All constructs were completely sequenced before use using an ABI Prism sequencer.

Cell Cultivation and Transfections—COS-7 (African green monkey kidney cells) and HeLa cells (both from ATCC (Manassas, VA)) were cultivated on plastic dishes or glass coverslips at 37 °C, 5% CO_2 in Dulbecco's modified Eagle's medium supplemented with Glutamax™ (Invitrogen), 10% fetal bovine serum (HyClone, Cramlington, UK) and penicillin/streptomycin (Sigma). One day after plating, cells were transfected using the FuGENE 6™ transfection reagent (Roche Applied Science) and 250 ng of each plasmid cDNA. One day later, the cells were fixed for indirect immunofluorescence, solubilized with SDS sample buffer for immunodetection on nitrocellulose membranes, or detached by trypsin-EDTA for quantification by flow cytometry (see below).

Indirect Immunofluorescence—To confirm the expression and Golgi localization of the different fusion constructs tagged with the full-length YFP or with its VN and VC terminal fragments, we followed the protocol used earlier for indirect immunofluorescence staining of fixed cells (37, 38). The following antibodies were used in the experiments. Polyclonal rabbit anti-GFP (1:1000 dilution; Affinity BioReagents (Golden, CO)) and goat anti-GFP (1:500; Santa Cruz Biotechnology, Inc. (Santa Cruz, CA)) antibodies were used for immunofluorescence detection of the expressed N-terminal (VN) and C-terminal (VC) YFP-fusion proteins, respectively. Monoclonal anti-c-Myc antibody (1:250; catalog no. sc-40, Santa Cruz Biotechnology, Inc.) was used for the detection of c-Myc-tagged constructs, and the anti-GM130 monoclonal antibody (1:250; catalog no. 610822, BD Biosciences) was used as a Golgi marker in co-localization studies. As secondary antibodies, Alexa fluor (488, 594, and 350)-conjugated goat anti-mouse, goat anti-rabbit, and donkey anti-goat antibodies (Invitrogen) were used at 1:1000 dilution. After fixation and staining, cells were photographed using an Olympus epifluorescence microscope equipped with a ×60 (numerical aperture 1.40) oil immersion objective; appropriate filter sets for YFP, TRITC, and 4′,6-diamidino-2-phenylindole; a CCD camera; and AnalySIS Pro 3.2 software (SoftImaging System, Inc., Lakewood, CO). The YFP filter set was used for the detection of the BiFC signal or the YFP protein itself, whereas the 4′,6-diamidino-2-phenylindole or TRITC filter sets with appropriate primary and secondary antibodies were used for the detection of the VN and VC terminal YFP fragments, the c-Myc epitope-tagged constructs, or the Golgi marker (GM130) in the transfected cells.

Quantification of the BiFC Signal by Flow Cytometry—Cells transfected for 24 h were washed with phosphate-buffered saline and harvested by trypsin-EDTA before centrifugation at 1000 rpm for 5 min. The cell pellet was then resuspended in phosphate-buffered saline, centrifuged again, and resuspended into 1.5 ml of phosphate-buffered saline. BiFC signal was measured using the CyFlow Space flow cytometer equipped with an appropriate filter set for YFP (Partec GmbH, Münster, Germany). In each case, 5000 cells were counted in triplicate (total

of 15,000 events/measurement) and used to calculate the average BiFC signal intensity ± S.D. ($n = 3$) in each sample using the FloMAX software. Full-length YFP fluorescence signal (obtained by transfecting cells with 250 ng of corresponding plasmid cDNA) was used as the interassay reference value (100%) for maximal fluorescence in each experiment, against which the BiFC signal intensities were normalized.

Immunodetection of Expressed Fusion Constructs—One day after transfection, cells were treated with 25 mM *N*-ethylmaleimide in phosphate-buffered saline for 10 min before lysis in SDS sample buffer, pH 6 (39). After SDS-PAGE, the proteins were electrophoretically transferred onto nitrocellulose membranes. The membrane was first quenched with 5% nonfat milk powder in Tris-buffered saline, pH 7.4, for 1–2 h at room temperature and incubated in the presence of appropriate primary and peroxidase-conjugated secondary antibodies. Monoclonal anti-GFP antibody (8362-1, BD Biosciences) was used at 1:5000 for visualization of VN, whereas the polyclonal goat anti-GFP antibody (Santa Cruz Biotechnology, Inc.) was used (1:2000 dilution) for the detection of the VC. ECL substrates (GE Healthcare) and exposure to Hyperfilm (GE Healthcare) were used for visualization of the antigens on the membrane. Image J 1.42k (National Institutes of Health) was used for quantification.

Statistical Analysis—Statistical analyses of data were performed using Student's *t* test. *p* values of <0.05 were considered significant.

RESULTS

For each of the four main human Golgi *N*-glycosyltransferases (Fig. 1*A*), we constructed four different BiFC constructs, whose schematic structures are shown in Fig. 1*B*. In our first BiFC measurements, we chose SiaT as our target because previous studies have shown that it forms disulfide-mediated homodimers (40, 41). We confirmed that both SiaT constructs (SiaT VN and SiaT VC) localized correctly in the Golgi membranes of COS-7 cells using domain-specific anti-GFP and Golgi marker (anti-GM130) antibodies (Fig. 1*C*). Subsequent transfections of the cells with 250 ng of either the SiaT VN or SiaT VC alone did not produce any detectable YFP fluorescence (BiFC signal) over the background (Fig. 2*A*). Similar results were obtained when the cells were co-transfected with the VN plasmid (without inserted SiaT) together with the SiaT VC construct (or *vice versa*; data not shown). However, when both SiaT VN and SiaT VC constructs were co-expressed, we obtained a clear BiFC signal both in COS-7 cells and in HeLa cells (Fig. 2*A*), indicating cell type-independent interactions. In both cases, BiFC signal was detected almost exclusively in the Golgi membranes of the cells. The measured BiFC signal intensities (mean ± S.D.) were 30.2 ± 3.1% of the maximal SiaT YFP fluorescence in COS-7 cells and 28.5 ± 5.4% in HeLa cells (Fig. 2, *B* and *C*). Both values are close to the theoretical maximum (33.33%) because only one (VN/VC) of the other two possible (VN/VN and VC/VC) SiaT homodimer combinations will result in the formation of fluorescent YFP protein. Based on the measured BiFC signal intensities (28.5–30.2% out of 33.3%), over 90% of the SiaT molecules appear to be homodimeric in the Golgi membranes of live cells. Background fluorescence

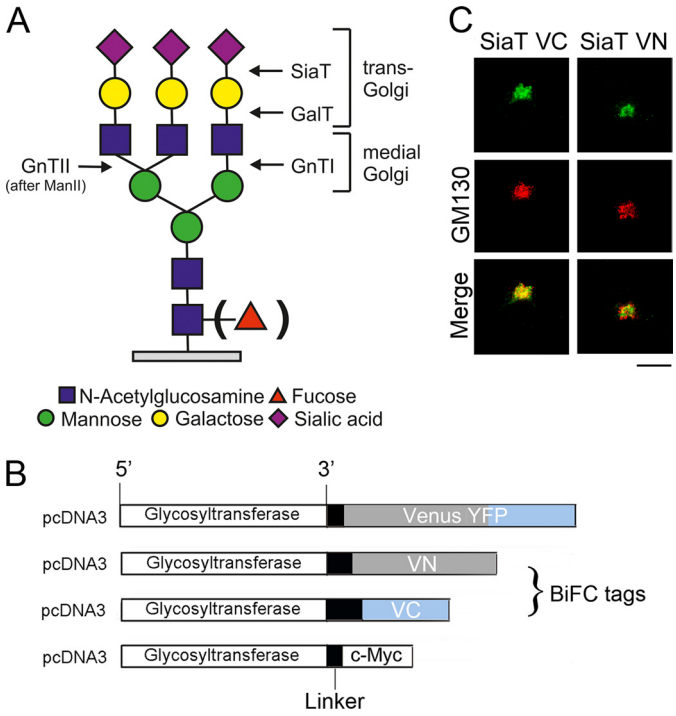

FIGURE 1. **Schematic representation of the *N*-glycosylation pathway with the main enzymes and the plasmid constructs used in the study.** *A*, a typical *N*-glycan structure and the sites where the four glycosyltransferases function during *N*-glycan synthesis. *B*, schematic view of the general structures of the glycosyltransferase constructs. Each enzyme's cDNA was amplified with PCR and inserted into the multiple cloning site of the four different pcDNA3 plasmids (see "Experimental Procedures"), each of which carried additional sequences encoding either the VN (*gray*) or VC (*blue*) fragments of the Venus YFP, the full-length YFP, or the c-Myc tag. The former two represent the BiFC constructs, whereas the latter two were used for the specificity controls for the BiFC assay. *C*, co-localization of the final SiaT BiFC constructs with the Golgi marker, GM130. Cells expressing the SiaT VN and VC constructs were fixed and stained with VN and VC fragment-specific antibodies (rabbit and goat anti-GFP antibodies, respectively; *green*), whereas the Golgi marker was visualized with the anti-GM130 antibody (*red*). *Scale bar*, 10 μm.

(measured from single transfectants or from non-transfected cells; data not shown) was always below 10% of the maximal YFP fluorescence.

To confirm that the observed BiFC signal is indeed dependent on SiaT homodimerization and not merely a consequence of complementation between the YFP fragments themselves, we co-expressed both competitive and non-competitive c-Myc-tagged protein constructs along with the SiaT VN and VC constructs. An equivalent amount of SiaT-Myc cDNA (250 ng) was found to reduce the BiFC signal by 47.9 ± 1.7% ($p < 0.001$; Fig. 2*D*). The amount of inhibition is in line with SiaT-Myc being able to interact with SiaT VN and/or VC constructs, thereby preventing their association and BiFC. Doubling the amount of SiaT-Myc cDNA (500 ng) reduced the signal to near background levels (86.3 ± 0.9% inhibition, $p < 0.001$). In contrast, co-expression of a c-Myc-tagged Golgi membrane protein AE2a (42) or c-Myc-tagged GnTII reduced the BiFC signal only by 7.6 ± 1.8% ($p > 0.05$) and 6.9 ± 2.2% ($p > 0.05$), respectively. c-Myc-tagged GalT, on the other hand, was found to reduce the BiFC signal by 36.6 ± 2.7%, ($p < 0.001$), probably due to its interaction with SiaT (see below). Thus, only SiaT itself (and, to a lesser extent, GalT) was able to inhibit BiFC between SiaT VN and SiaT VC. This demonstrates that

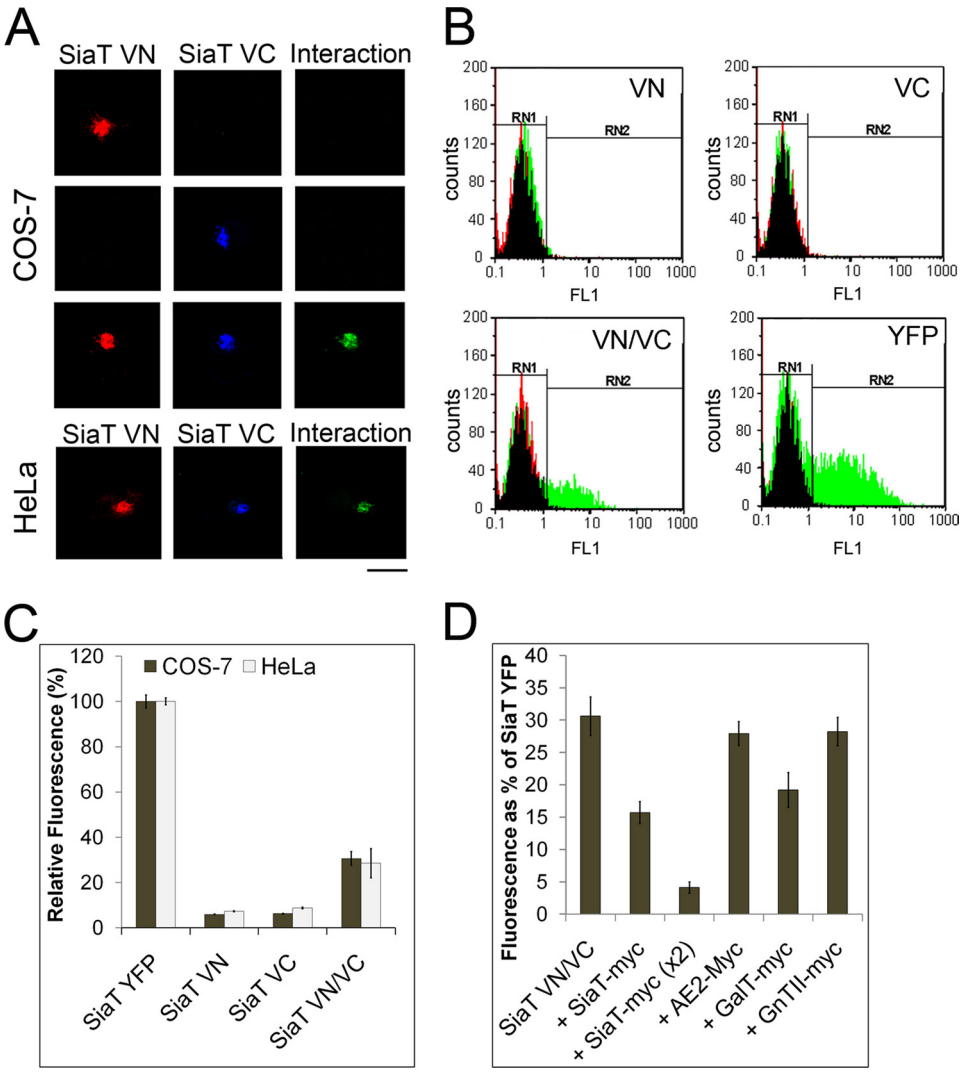

FIGURE 2. **Formation of SiaT homodimers in live cells.** *A*, detection of BiFC signal with fluorescence microscopy. COS-7 cells were transfected either with SiaT VN (*top row*) or SiaT VC (*middle row*) alone or with SiaT VN and VC together (*bottom row*). One day after transfection, cells were fixed and stained with BiFC fragment-specific antibodies and appropriate Alexa Fluor-conjugated secondary antibodies. Cells were imaged using specific filter sets for VN (*red*) and VC (*blue*), whereas the BiFC signal (*green fluorescence*) was detected using the YFP filter set. Each row corresponds to a single cell. Note that SiaT homodimers (BiFC signal) were detected only when the two BiFC constructs were co-transfected together. Similar results were obtained with HeLa cells. *Scale bar*, 10 μm. *B*, flow cytometric quantification of the BiFC signal. Shown are representative runs after transfecting cells with either the SiaT VN and VC plasmids alone or in combination or with only the full-length SiaT YFP-encoding plasmid (250 ng of plasmid per cDNA). In each case, BiFC signal intensities (*green*) were measured in the gated area RN2. The fluorescence in the RN1 area (*red*) represents background fluorescence (autofluorescence). *C* and *D*, column diagrams of the measured BiFC signal intensities in COS-7 and HeLa cells. Each *column* represents the mean ± S.D. (*error bars*) of three independent experiments (5000 cells/experiment) expressed as percentages of the signal intensity obtained with an equivalent amount (250 ng) of the full-length SiaT YFP-encoding plasmid. Note that no BiFC signal was obtained with single transfectants and that co-transfection of only competitive c-Myc-tagged SiaT and GalT constructs reduced the BiFC signal markedly. The *plus signs* in *D* denote the competing or non-competing protein constructs that were co-transfected along with the SiaT VN and VC constructs.

homodimerization of SiaT is indeed driven by the enzyme domains of the two BiFC constructs.

Homodimerization of SiaT was confirmed by immunodetection of SDS-PAGE-resolved proteins. Fig. 3*A* shows that, under non-reducing conditions, all of the different SiaT constructs (SiaT YFP, SiaT VN, and SiaT VC) migrated on SDS-PAGE both as monomers (67.5 and 74 kDa bands) and higher molecular mass dimers (126–148 kDa) or oligomers (~200 kDa). Dimers and oligomers comprised 30–40% of the total SiaT in each sample, regardless of the tag used. Reduction of the samples with DTT (Fig. 3*B*) resulted in the disappearance of the dimers and oligomers, consistent with the observed disulfide-mediated homodimerization of rat SiaT (40, 41). Mutation of the critical cysteine (C24G) within the transmembrane domain of human SiaT, which is known to abolish disulfide-mediated dimerization of rat SiaT (31), however, did not interfere with either the correct Golgi localization (Fig. 3*C*), or the homodimerization of SiaT in live cells (Fig. 3, *C* and *D*). The measured BiFC signal for the C24G mutant (27.9 ± 1.6%) was comparable with that of the wild type SiaT (30.2 ± 3.1%). The BiFC signal was also markedly reduced by co-expressing c-Myc-tagged SiaT (39.0 ± 4.1% inhibition, $p < 0.01$) but not by c-Myc-tagged AE2 (8.6 ± 0.9% inhibition, $p > 0.01$). Thus, in addition to disulfide bonds, SiaT homodimerization in live cells also seems to involve non-covalent interactions.

Homodimerization of the more proximal *N*-glycosyltransferases (Fig. 1*A*) was examined next. Co-expression of the GalT VN and VC constructs resulted in a prominent BiFC signal (25.8 ± 3.6% of the full-length YFP fluorescence) in the Golgi membranes of live cells (Fig. 4, *A* and *B*). The signal with single transfectants was below 10% in both cases. GalT homodimerization was also inhibited by co-expression with the c-Myc-tagged GalT by 35.6 ± 4.5% ($p < 0.01$) but not by c-Myc-tagged AE2 (−1.6 ± 0.7%, $p > 0.05$). Thus, GalT, like SiaT, forms Golgi-localized homodimers in live cells.

BiFC measurements with the medial Golgi enzymes GnTI and GnTII gave similar results. Co-expression of the GnTI VN and VC (Fig. 4, *A* and *C*) or GnTII VN and VC constructs (Fig. 4, *A* and *D*) resulted in a detectable BiFC signal, although the signal was somewhat lower with GnTI than with GnTII (17.3 ± 1.3 and 29.9 ± 1.5% of the full-length YFP fluorescence, respectively). This is probably due to poorer folding of the GnTI, as suggested by its more prevalent presence in the ER of the transfected cells (data not shown). Nevertheless, the BiFC signal with GnTI was detected only in the Golgi membranes of live cells (Fig. 4*A*). In either case, the

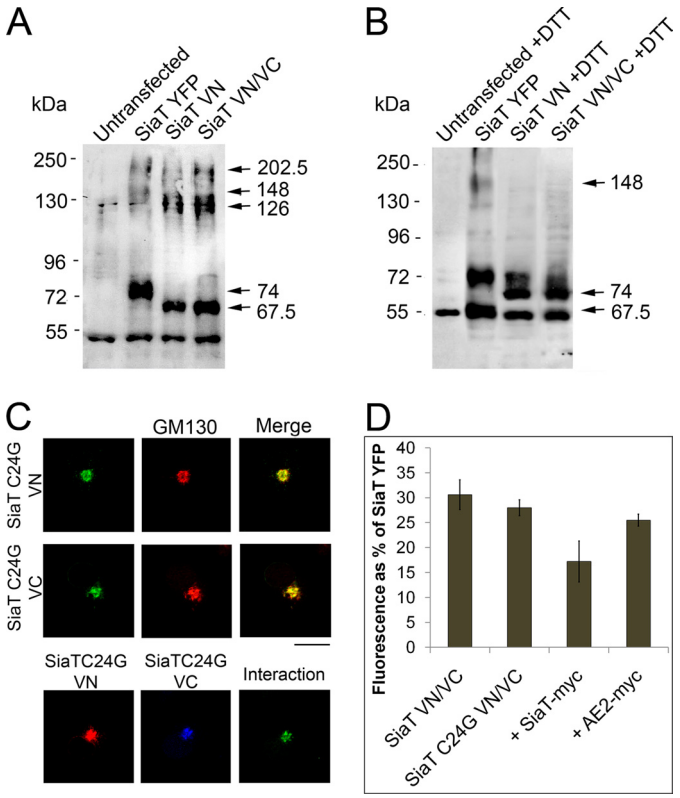

FIGURE 3. **Visualization of SiaT homodimers by immunodetection.** *A* and *B*, single- or double-transfected cells were solubilized directly in SDS sample buffer and subjected to SDS-PAGE under non-reducing (*A*) or reducing (*B*) conditions before transfer onto the nitrocellulose filter. For immunodetection of the constructs, the anti-N-terminal GFP antibodies were used. Note that all of the SiaT constructs migrated as monomers (67.5 and 74 kDa), homodimers (126 and 148 kDa), and oligomers (>200 kDa) on SDS-PAGE under non-reducing conditions (*A*) but only as monomers under reducing conditions (*B*). The SiaT YFP construct served as a control and was not treated with DTT. *C*, localization of the BiFC constructs of the SiaT cysteine mutant (C24G). After single transfections, cells were fixed and stained with the fragment-specific antibodies. Note the co-localization of the constructs (*green*) with the Golgi marker (GM130; *red*), and the BiFC signal (*bottom*) after co-transfecting the cells with the VN and VC constructs. *Scale bar*, 10 μm. *D*, quantification of the BiFC signals by flow cytometry. Signal intensities were measured by flow cytometry as described above. Note that the BiFC signal of the mutant construct was comparable with that of the wild-type SiaT construct and was also inhibited by the c-Myc-tagged SiaT. *Error bars*, S.D.

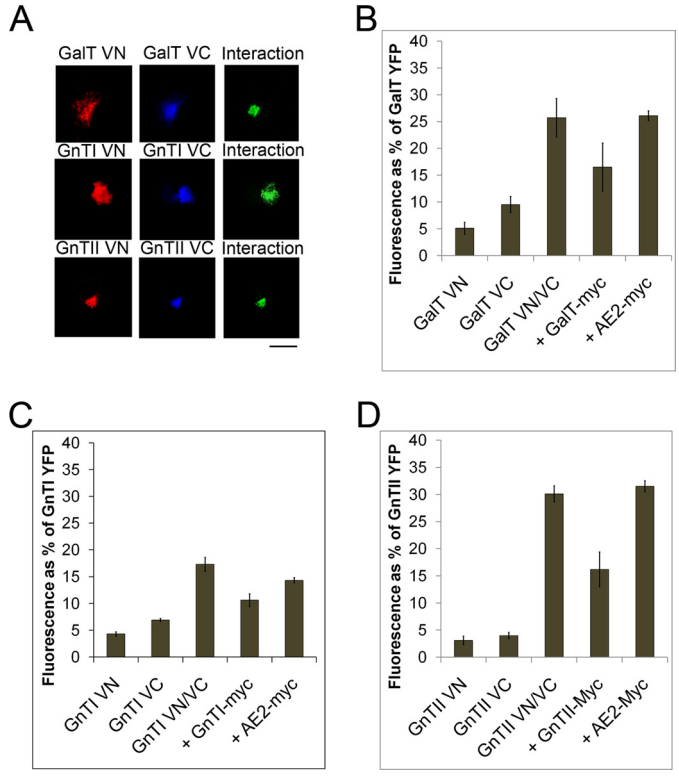

FIGURE 4. **Homodimerization of other Golgi *N*-glycosyltransferases in live cells.** *A*, visualization of the BiFC signal by fluorescence microscopy. Cells co-transfected with the relevant VN and VC constructs of the different enzymes tested (GalT, GnTI, and GnTII) were fixed, stained with fragment-specific antibodies, and visualized with appropriate secondary antibodies (*red* and *blue*) as above. The YFP filter set was used to visualize the BiFC signal if present. *Scale bar*, 10 μm. *B–D*, quantification of the BiFC signal of the different enzyme constructs (GalT (*B*), GnTI (*C*), and GnTII (*D*)) by flow cytometry. Quantification was performed as described above. The signal intensities are expressed as percentages of the signal obtained with the full-length YFP construct of each enzyme. *Error bars*, S.D.

BiFC signal was also markedly reduced by co-expression of the c-Myc-tagged constructs along with the BiFC constructs. For GnTI, the inhibition was 38.8 ± 1.2% ($p < 0.01$), and for GnTII, it was 46.1 ± 1.2% ($p < 0.001$), confirming the specificity of the interaction. Reduction with the c-Myc-tagged AE2 was much less marked or non-existent (17.7 ± 0.5% ($p < 0.05$) and 2.1 ± 1.1% ($p > 0.05$), respectively). Thus, in addition to the *trans*-Golgi enzymes SiaT and GalT, the medial Golgi enzymes GnTI and GnTII also assemble into Golgi-localized homodimers in live cells. Unfortunately, we could not assess the homodimerization of mannosidase II due to severe folding problems faced with its BiFC constructs.

By using the ER retrieval assay (26, 43), the medial Golgi enzymes GnTI, GnTII, and mannosidase II (but not the *trans*-Golgi enzymes GalT and SiaT) have been shown to form "kin" heterodimers. Therefore, we utilized BiFC to screen any such potential interactions between the four consecutively acting glycosyltransferases in the Golgi membranes of live cells. Co-expression of the GnTI VN construct with the GnTII VC construct resulted in a prominent BiFC signal (30.2 ± 1.3% of the full-length GnTI YFP construct; Fig. 5*A*) in the Golgi membranes of live cells. Reversal of the tags (GnTI VC and GnTII VN) gave similar results (data not shown). Co-expression of the c-Myc-tagged GnTII construct also markedly reduced the BiFC signal (by 31.8 ± 1.6%, $p < 0.001$), whereas AE2-Myc did not (3.4 ± 0.3%, $p < 0.001$). These results show, for the first time, that the two medial Golgi enzymes also form heterodimers in the Golgi membranes of live cells.

In contrast to previous findings, our microscopic analyses revealed a clear interaction between the *trans*-Golgi enzymes GalT VC and SiaT VN (Fig. 5*B*). Co-expression of the constructs with reversed tags (GalT VN and SiaT VC) gave similar results. However, neither SiaT (Fig. 5*B*), nor GalT (data not shown) was found to interact with the medial Golgi enzyme GnTII. Flow cytometric quantification (Fig. 5*C*) revealed a clear BiFC signal (30.2 ± 1.3%) for the GalT·SiaT heterodimer, whereas no BiFC signal was detected between SiaT and GnTII or between GalT and GnTII (7.3 ± 0.4 and 6.3 ± 0.6% of the full-length SiaT YFP fluorescence, respectively). Similar results were obtained with both tag combinations used. Heterodimerization between SiaT and GalT (Fig. 5*C*) was also inhibited by co-expression of the c-Myc-tagged SiaT (50.7 ± 1.2%, $p <$

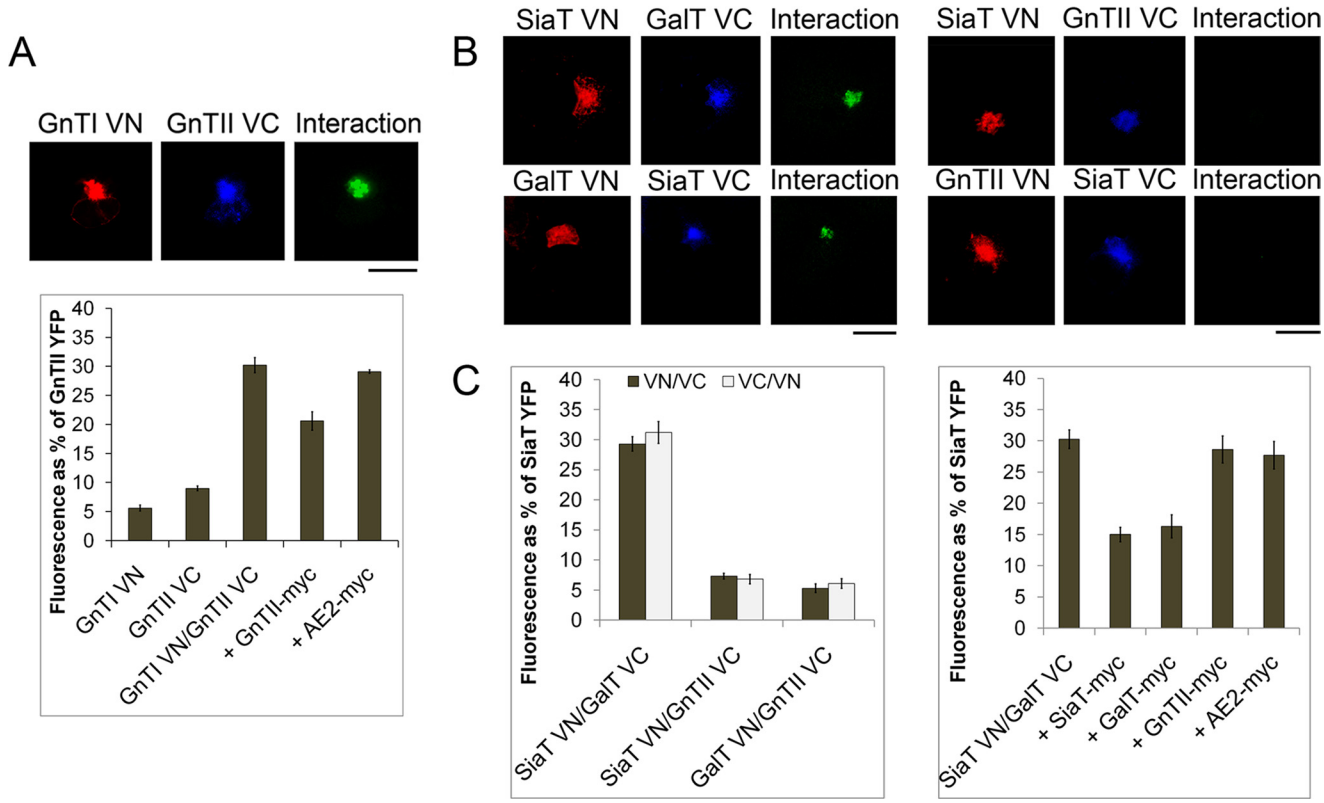

FIGURE 5. **Formation of heterodimers between medial Golgi and *trans*-Golgi *N*-glycosyltransferases.** *A*, immunofluorescence detection and flow cytometric quantification of the BiFC signals between the medial Golgi enzymes GnTI and GnTII. Note the interaction (*green*) only in double (with both VN and VC) transfectants and that the interaction is inhibited by the c-Myc-tagged GnTII (and GnTI; data not shown) but not by the c-Myc-tagged AE2 construct. The cells were prepared for immunofluorescence detection and quantification by flow cytometry as described above. *Scale bar*, 10 μm. *B*, detection of heterodimers between the *trans*-Golgi enzymes SiaT and GalT by fluorescence microscopy. Cells were prepared for microscopy as described above. Note the BiFC signal between SiaT and GalT (*green*, *left*) and the absence of signal between SiaT and GnTII (*right*). Similar results were obtained by reversal of the BiFC tags. *Scale bar*, 10 μm. *C*, flow cytometric quantification of heterodimerization between SiaT, GalT, and GnTII enzyme constructs. Quantification of the BiFC signal was performed as described above. Note the heterodimerization between SiaT and GalT with both BiFC tag combinations used (*left*). Heterodimerization was also inhibited by both SiaT-Myc and GalT-Myc, whereas GnTII-Myc and AE2-Myc had no effect (*right*). *Error bars*, S.D.

0.001) or c-Myc-tagged GalT (45.8 ± 1.9%, $p < 0.001$) but not with c-Myc-tagged GnTII and AE2 (5.5 ± 2.2% ($p > 0.05$) and 8.2 ± 2.1% ($p > 0.01$)). Thus, in contrast to earlier studies, our results show that the two *trans*-Golgi enzymes also assemble into Golgi-localized heterodimers in live cells. Because neither of the *trans*-Golgi enzymes tested interacted with the medial Golgi enzyme GnTII, the GalT-SiaT heterodimer appears to be distinct from the GnTI-GnTII heterodimer.

DISCUSSION

The above findings are generally consistent with the previous data obtained from *in vitro* pull-down experiments and from the *in vivo* ER retrieval assays. Both of these approaches have separately demonstrated the existence of certain glycosyltransferase homo- or heterodimers and, in some cases, enzyme oligomers (23, 40, 43, 44). However, our results are the first to emphasize that *N*-glycosyltransferases in general tend to form enzyme complexes in live cells and that the complexes localize almost exclusively in the Golgi membranes (*i.e.* the site where they are known to function). Most importantly, our results show that *N*-glycosyltransferases not only form homodimers but also are able to assemble into functionally relevant heterodimers, one in the medial Golgi (GnTI and GnTII) and the other in the *trans*-Golgi (GalT and SiaT). Although the former appears to be identical to the medial Golgi complex identified previously and probably also includes mannosidase II (26), the latter represents a previously unknown heterodimer that has not been detected by other methods (27, 43), despite their observed co-localization in the cells (45, 46). This probably reflects the ability of BiFC to detect even weak ion- or pH-dependent interactions in the slightly acidic environment of the Golgi lumen. In support of this view, rat SiaT oligomers exhibit different solubilities at pH 8 and at the physiological pH (pH 6) of the Golgi lumen (28).

Given their sequential action and strict Golgi localization, the two distinct heterodimers identified in this study are probably responsible for the processing and maturation of *N*-glycans in live cells. The medial Golgi enzyme complex (GnTI, GnTII, and mannosidase II) is predicted to be responsible for the trimming of high mannose *N*-glycans into hybrid and complex glycans, whereas the *trans*-Golgi GalT·SiaT complex is probably involved in the termination of glycan chains. This suggested two-step *N*-glycan synthesis model is reminiscent of the *N*-glycosylation pathway of *Saccharomyces cerevisiae*, in which two different enzyme complexes, termed M-Pol I and M-Pol II (47), are known to be responsible for the synthesis of core structures of high mannose type glycans. In addition, two distinct enzyme complexes appear to be involved in the synthesis of

gangliosides (48, 49) and heparan sulfate (19, 50). In the latter cases, complex formation has also been shown to correlate either with the full enzymatic activity of the complex constituents or with the correct glycosylation of the substrates (20). The only exception to this two-step synthesis model appears to be the *O*-glycosylation pathway, for which direct *in vivo* evidence for the existence of similar enzyme complexes is currently lacking but should now be amenable to assessment by BiFC. Further work is necessary to delineate the functional relevance of the observed enzyme homodimers, but one obvious role for them could be to eliminate excess enzyme from productive glycosylation processes in the absence of a functionally relevant enzyme partner. This is consistent with the observed competition between the formation of enzyme homo- and heterodimers (Figs. 2*C* and 5*D*). Multicolor BiFC will be helpful in determining whether this scenario is correct or not and to directly assess whether it is homodimerization or heterodimerization that is the preferred interaction between *N*-glycosyltransferases in live cells. Finally, a better understanding of the supramolecular organization of the different Golgi glycosylation pathways will help to shed light on how the Golgi glycosylation machinery actually functions in higher eukaryotes and why it is defective in certain disease states, such as cancer.

Acknowledgments—We thank Dr. Chang-Deng Hu (Purdue University) for providing the original BiFC vectors. Dr. Nina Kokkonen is acknowledged for carefully reading the manuscript.

REFERENCES

1. Paulson, J. C. (1989) *Trends Biochem. Sci.* **14,** 272–276
2. Varki, A. (1993) *Glycobiology* **3,** 97–130
3. Ohtsubo, K., and Marth, J. D. (2006) *Cell* **126,** 855–867
4. Rabinovich, G. A., and Toscano, M. A. (2009) *Nat. Rev. Immunol.* **9,** 338–352
5. Dennis, J. W., Granovsky, M., and Warren, C. E. (1999) *BioEssays* **21,** 412–421
6. Freeze, H. H. (2001) *Glycobiology* **11,** 37G–38G
7. Grunewald, S., Matthijs, G., and Jaeken, J. (2002) *Pediatr. Res.* **52,** 618–624
8. Ungar, D. (2009) *Semin. Cell Dev. Biol.* **20,** 762–769
9. Farquhar, M. G., and Palade, G. E. (1981) *J. Cell Biol.* **91,** 77s–103s
10. Dunphy, W. G., Fries, E., Urbani, L. J., and Rothman, J. E. (1981) *Proc. Natl. Acad. Sci. U.S.A.* **78,** 7453–7457
11. Warren, G., and Malhotra, V. (1998) *Curr. Opin. Cell Biol.* **10,** 493–498
12. Glick, B. S. (2000) *Curr. Opin. Cell Biol.* **12,** 450–456
13. Roth, J., and Berger, E. G. (1982) *J. Cell Biol.* **93,** 223–229
14. Dunphy, W. G., and Rothman, J. E. (1985) *Cell* **42,** 13–21
15. Kornfeld, R., and Kornfeld, S. (1985) *Annu. Rev. Biochem.* **54,** 631–664
16. Roth, J. (2002) *Chem. Rev.* **102,** 285–303
17. Schachter, H. (1986) *Biochem. Cell Biol.* **64,** 163–181
18. Gleeson, P. A. (1998) *Histochem. Cell Biol.* **109,** 517–532
19. Pinhal, M. A., Smith, B., Olson, S., Aikawa, J., Kimata, K., and Esko, J. D. (2001) *Proc. Natl. Acad. Sci. U.S.A.* **98,** 12984–12989
20. de Graffenried, C. L., and Bertozzi, C. R. (2004) *Curr. Opin. Cell Biol.* **16,** 356–63
21. Young, W. W., Jr. (2004) *J. Membr. Biol.* **198,** 1–13
22. Noffz, C., Keppler-Ross, S., and Dean, N. (2009) *Glycobiology* **19,** 472–478
23. Nilsson, T., Slusarewicz, P., Hoe, M. H., and Warren, G. (1993) *FEBS Lett.* **330,** 1–4
24. Weisz, O. A., Swift, A. M., and Machamer, C. E. (1993) *J. Cell Biol.* **122,** 1185–96
25. Colley, K. J. (1997) *Glycobiology* **7,** 1–13
26. Nilsson, T., Hoe, M. H., Slusarewicz, P., Rabouille, C., Watson, R., Hunte, F., Watzele, G., Berger, E. G., and Warren, G. (1994) *EMBO J.* **13,** 562–574
27. Opat, A. S., Houghton, F., and Gleeson, P. A. (2000) *J. Biol. Chem.* **275,** 11836–11845
28. Chen, C., Ma, J., Lazic, A., Backovic, M., and Colley, K. J. (2000) *J. Biol. Chem.* **275,** 13819–13826
29. Axelsson, M. A., Karlsson, N. G., Steel, D. M., Ouwendijk, J., Nilsson, T., and Hansson, G. C. (2001) *Glycobiology* **11,** 633–44
30. Schaub, B. E., Berger, B., Berger, E. G., and Rohrer, J. (2006) *Mol. Biol. Cell* **17,** 5153–62
31. Rivinoja, A., Hassinen, A., Kokkonen, N., Kauppila, A., and Kellokumpu, S. (2009) *J. Cell. Physiol.* **220,** 144–54
32. Hu, C. D., Chinenov, Y., and Kerppola, T. K. (2002) *Mol. Cell* **9,** 789–798
33. Galarneau, A., Primeau, M., Trudeau, L. E., and Michnick, S. W. (2002) *Nat. Biotechnol.* **20,** 619–622
34. Nyfeler, B., Michnick, S. W., and Hauri, H. P. (2005) *Proc. Natl. Acad. Sci. U.S.A.* **102,** 6350–6355
35. Shyu, Y. J., Liu, H., Deng, X., and Hu, C. D. (2006) *BioTechniques* **40,** 61–66
36. Yang, W., and Storrie, B. (1997) *Cell Biol. Int.* **21,** 223–228
37. Kokkonen, N., Rivinoja, A., Kauppila, A., Suokas, M., Kellokumpu, I., and Kellokumpu, S. (2004) *J. Biol. Chem.* **279,** 39982–39988
38. Rivinoja, A., Kokkonen, N., Kellokumpu, I., and Kellokumpu, S. (2006) *J. Cell. Physiol.* **208,** 167–174
39. Molinari, M., and Helenius, A. (1999) *Nature* **402,** 90–93
40. Ma, J., and Colley, K. J. (1996) *J. Biol. Chem.* **271,** 7758–7766
41. Fenteany, F. H., and Colley, K. J. (2005) *J. Biol. Chem.* **280,** 5423–29
42. Holappa, K., Suokas, M., Soininen, P., and Kellokumpu, S. (2001) *J. Histochem. Cytochem.* **49,** 259–269
43. Munro, S. (1995) *EMBO J.* **14,** 4695–4704
44. Teasdale, R. D., Matheson, F., and Gleeson, P. A. (1994) *Glycobiology* **4,** 917–928
45. Nilsson, T., Pypaert, M., Hoe, M. H., Slusarewicz, P., Berger, E. G., and Warren, G. (1993) *J. Cell Biol.* **120,** 5–13
46. Rabouille, C., Hui, N., Hunte, F., Kieckbusch, R., Berger, E. G., Warren, G., and Nilsson, T. (1995) *J. Cell Sci.* **108,** 1617–1627
47. Jungmann, J., and Munro, S. (1998) *EMBO J.* **17,** 423–434
48. Giraudo, C. G., Daniotti, J. L., and Maccioni, H. J. (2001) *Proc. Natl. Acad. Sci. U.S.A.* **98,** 1625–1630
49. Giraudo, C. G., and Maccioni, H. J. F. (2003) *J. Biol. Chem.* **278,** 40262–71
50. McCormick, C., Duncan, G., Goutsos, K. T., and Tufaro, F. (2000) *Proc. Natl. Acad. Sci. U.S.A.* **97,** 668–673